Remote Sensing of Environment 140 (2014) 233–240

Contents lists available at ScienceDirect

Remote Sensing of Environment

journal homepage: www.elsevier.com/locate/rse

Assessment of smoke shortwave radiative forcing using empirical angular distribution models

Falguni Patadia [a], Sundar A. Christopher [b,*]

[a] Goddard Earth Science and Technology Center, MD, United States
[b] The University of Alabama in Huntsville, Huntsville, AL, United States

ARTICLE INFO

Article history:
Received 9 April 2013
Received in revised form 15 August 2013
Accepted 17 August 2013
Available online 27 September 2013

Keywords:
Aerosol
Biomass burning
Climate
Radiative forcing

ABSTRACT

The Clouds and the Earth's Radiant Energy System (CERES) data has been used by several studies to calculate the top of atmosphere (TOA) shortwave aerosol radiative forcing (SWARF) of biomass burning aerosols over land. However, the current CERES angular distribution models that are used to convert measured TOA radiances to fluxes are not characterized by aerosols. Using our newly developed empirical angular models for smoke aerosols we calculate the SWARF over South America for eight years (2000–2008) during the biomass burning season. Our results indicate that when compared to our new angular distribution model-derived values, the instantaneous SWARF is underestimated by the CERES data by nearly 3.3 Wm^{-2}. Our studies indicate that it is feasible to develop angular models using empirical methods that can then be used to reduce uncertainties in aerosol radiative forcing calculations. More importantly, empirically-based methods for calculating radiative forcing can serve as a benchmark for modeling studies.

1. Introduction

Biomass burning is a major source of tropospheric aerosols. Nearly 80% of all biomass burning takes place in the tropics (Hao & Liu, 1994; Ito & Penner, 2004), largely due to agricultural burning (Crutzen & Andreae, 1990; Vermote et al., 2009) and producing more than 100 teragrams of aerosols. Biomass burning in South America constitutes almost 30% of the world's total activities (Guyon et al., 2005) and about half of this is transported over long distances (Andreae et al., 2001) and dominates the carbonaceous aerosol load in the southern hemisphere (Koch, Bond, Streets, & Unger, 2007). These aerosols modify the radiation balance of the earth–atmosphere system through different mechanisms. Through the direct effect, they scatter and absorb the incoming solar radiation thereby reducing the amount of solar radiation reaching the ground or by redistributing energy through the atmosphere (Haywood & Boucher, 2000). Through the indirect effect, they also modify cloud properties, change rainfall patterns and alter lifetime of clouds (Ackerman et al., 2000; Jones & Christopher, 2010; Kaufman & Fraser, 1997; Marengo, Jones, Alves, & Valverde, 2009; Reid, Hobbs, Rangno, & Hegg, 1999; Rosenfeld & Woodley, 2000). Due to absorption of solar radiation, smoke aerosols also heat the tropospheric air column (Koren, Kaufman, Remer, & Martins, 2004) thereby changing atmospheric circulation patterns (Zhang et al., 2009) and surface processes (Moraes, Franchito, & Brahmananda Rao, 2004). It is therefore important to study the direct and indirect aerosol effects because of its significant role on the Earth's climate (CCSP, 2009; IPCC, 2007).

The radiative effect of biomass burning aerosols is usually described in terms of top of atmosphere (TOA) shortwave aerosol radiative forcing (SWARF) that is defined as the change in the reflected radiative flux between clear and aerosol skies (e.g. Christopher, Chou, et al., 2000). Since biomass-burning aerosols are largely dominated by sub-micron fine mode particles, their impact in the longwave is negligible (Kaufman et al., 2000). Observation based methods of calculating SWARF have been reported in several studies (e.g. Yu et al., 2006). There are many empirical approaches for calculating the radiative forcing of biomass burning aerosols. These calculations have been made from (1) surface measurements (e.g. AERONET) coupled with radiative transfer (RT) calculations (e.g. Procopio et al., 2004), (2) in situ aircraft measurements (e.g. Bergstrom, Pilewskie, Schmid, & Russell, 2003), (3) satellite observations coupled with radiative transfer calculations (e.g. Ichoku et al., 2003), and (4) broadband satellite observations such as the Earth Radiation Budget Experiment (ERBE) or Clouds and the Earth's Radiant Energy System (CERES) (e.g. Christopher, Chou, et al., 2000; Christopher, Kliche, Chou, & Welch, 1996). Global models have also been used to calculate smoke aerosol forcing (e.g. Iacobellis, Frouin, & Somerville, 1999).

Since SWARF is the radiative impact across the entire solar spectrum ranging from approximately 0.2–4 μm, for methods that require detailed radiative transfer (RT) calculations, wavelength dependent information of aerosol optical depth, single scattering albedo (ω_0), and asymmetry parameter (g) are required. These calculations also need other information on surface albedo (α_s) and meteorological conditions such as vertical distribution of temperature and water vapor. Some studies provide SWARF for cloud-free conditions whereas others

* Corresponding author at: 301 Sparkman Drive, Huntsville, AL 35899, United States. Tel.: +1 256 961 7872.
E-mail address: sundar@nsstc.uah.edu (S.A. Christopher).

0034-4257/$ – see front matter © 2013 Elsevier Inc. All rights reserved.
http://dx.doi.org/10.1016/j.rse.2013.08.034

account for clouds by scaling the cloud-free values by appropriate cloud cover (Ross, Hobbs, & Holben, 1998). Further complications arise during these comparisons because some studies report SWARF for instantaneous conditions for a fixed solar zenith angle (Christopher et al., 1996) while others use an approximation to convert instantaneous SWARF to diurnally averaged values (Procopio et al., 2004; Zhang, Christopher, Remer, & Kaufman, 2005b).

Examples of satellite broadband observations are from the ERBE and CERES instruments where broadband radiance ($Wm^{-2}\ sr^{-1}$) measurements are made in the entire shortwave rather than in narrow wavelength intervals (Wielicki et al., 1996). The radiance measurements are converted to TOA shortwave (SW) (0.3–5 μm) fluxes using angular distribution models called ADMs (Loeb & Manalo-Smith, 2005; Wielicki et al., 1996; Zhang, Christopher, Remer, & Kaufman, 2005a). Comprehensive ADMs have been developed for surface and cloud conditions in the CERES data stream (Loeb & Manalo-Smith, 2005) but not for aerosols. One of the problems is due to the large footprint of CERES where accurate aerosol identification is not possible; therefore smoke aerosols are identified using 'narrowband' observations (e.g. Moderate resolution Imaging Spectroradiometer MODIS) and then the SWARF is obtained by using the CERES fluxes (e.g. Patadia, Gupta, Christopher, & Reid, 2008).

Prior studies have directly used the CERES fluxes from pixel level data to estimate the SWARF of biomass burning aerosols (Patadia et al., 2008). To accurately convert the CERES radiances to fluxes angular models that account for the anisotropy of the scene are necessary (Li, Christopher, Chou, & Welch, 2000; Zhang et al., 2005a). However, over land, the current CERES data sets do not use aerosol ADMs to convert the radiances to fluxes. To improve upon the current CERES shortwave flux calculations over biomass burning regions with high concentrations of smoke aerosols, we developed empirical smoke ADMs that are described in Patadia, Christopher, and Zhang (2011). A prior study used radiative transfer calculations with a range of biomass burning aerosol properties to calculate smoke ADMs (Li et al., 2000) and reported that when theoretical smoke ADMs were used, the difference between the SWARF estimated from the two datasets was nearly 10 Wm^{-2}. With the launch of the CERES with instruments that operated in several modes including the rotating azimuth plane, Patadia et al. (2011) developed empirical angular models from CERES data for biomass burning aerosols in the Amazon. The cloud free empirical angular distribution models (EADMs) developed as part of the current study further used AOT information from MODIS to quantify forcing efficiencies. Patadia et al. (2011) showed that the shortwave radiative flux available from the CERES data set is different from the shortwave flux derived using the empirical angular distribution models. These differences have implications for the observation-based estimates of shortwave aerosol radiative forcing. In this paper, an evaluation of the instantaneous shortwave aerosol radiative forcing (SWARF) calculated from the two shortwave flux datasets (i.e. from CERES–SSF and from our EADM) is presented. We further compare our results with prior work. Such comparisons and studies are needed since one of the goals of the CERES project when it was conceived was to develop empirical angular models to convert the radiances to fluxes thereby reducing the assumptions and uncertainties in the final radiative forcing products.

2. Data and methods

A brief description of the data sets used for SWARF estimation is presented here for the sake of completeness, but the reader is referred to Patadia et al. (2011) for a more complete description. The area of study is within 0–20°S and 40–70°W in South America, where biomass burning is prevalent during the dry season (August–October) (e.g. Bevan, North, Grey, Los, & Plummer, 2009; Ito & Penner, 2004; Prins, Feltz, Menzel, & Ward, 1998). Empirically-calculated SWARF requires observations of reflected solar radiative flux in conjunction with aerosol measurements so that the change in radiative fluxes due to aerosols can be analyzed. The SWARF is defined as the difference in the radiative fluxes in the absence and presence of aerosols (e.g. Patadia et al., 2008). The MODIS mid-visible AOT in the pixel level CERES product, which is the point spread function weighted (PSF-WTD) value in the CERES footprint, is used to identify the presence of aerosols. The CERES–SSF product contains the collection 4 MODIS AOT. The shortwave radiative flux information is used from two sources: (1) Shortwave flux from CERES SSF product and (2) Shortwave flux derived using empirical ADMs (Patadia et al., 2011). The CERES SSF product used in this study is the Edition2B_Rev1 Single Scanner Footprint TOA/Surface Fluxes and Clouds (SSF) product (Geier et al., 2001). Apart from the fluxes in shortwave, the SSF product also contains radiative fluxes in two other channels of the CERES instrument (window (8–12 μm) and total (0.2–100 μm) channels). There are four CERES instruments, two each onboard Terra (Flight Models 1 and 2) and Aqua (Flight Models 1 and 2) satellites. The CERES SSF product combines radiation measurements from the CERES instruments with simultaneous measurements of scene information (e.g. cloud and aerosol property) from MODIS on Terra and Aqua respectively. At the time the analysis for this paper was conducted, the CERES–SSF product contained the collection 4 MODIS AOT. All available CERES SSF from August–October of 2000–2008 are used in this study. Cloud cover information from the CERES SSF product (see Gupta, Patadia, & Christopher, 2008) is used to remove cloudy pixels. Data with cloud fraction greater than 99.5% is flagged as cloudy and is eliminated. For every 0.5×0.5 degree latitude–longitude grid, a regression relation is formed between the AOT and shortwave flux data in the grid. The y-intercept of regression relation gives the clear sky flux value (e.g. Patadia et al., 2008). The robustness of this technique is fully detailed in Patadia et al. (2008).

Two different forcing values are obtained from the two shortwave flux data sets mentioned above. In the rest of the paper, the SWARF calculated using CERES-shortwave flux will be referred to as SWARF–CADM and SWARF derived from our new angular models (Patadia et al., 2011) will be referred to as SWARF–EADM. To facilitate inter-comparison of the forcing from the two data sets, the calculations are done for the same pixels.

3. Results and discussion

The results are organized as follows. We first show the spatial distribution of aerosols from Terra–MODIS over the area of study and compare the MODIS AOT values used in this study with the AERONET retrievals that are widely considered as the standard for AOT assessments. We then show the spatial distribution of SWARF calculated using the CERES data and those derived from our empirical methods. Then, the relationship of SWARF with aerosol optical depth (forcing efficiency) from both methods is assessed. A comparison of our results with previous studies is then presented.

3.1. Inter-comparison of aerosol optical thickness

The new empirical angular distribution models developed in Patadia et al. (2011) are characterized by the point spread function weighted MODIS aerosol optical thickness. Since the CERES footprint is larger than that of MODIS, the CERES pixel level products use point spread function (PSF) weighting to convolve the MODIS AOT values into the CERES pixel. These AOT values are used to calculate the SWARF in this paper and therefore are not the same as the level 2 MODIS AOT data. We evaluate the representativeness of this data by comparing it against ground based AOT retrievals from AERONET. Fig. 1 shows the comparison between AERONET AOT and the PSF-weighted MODIS AOT. The map shows an 8 year (2000–2008) seasonal (August–October) composite of the spatial distribution of AOT in the study region. Note that our comparisons are all done for AOT within the CERES footprint and are therefore different than other comparisons of the level 2 MODIS aerosol products (Levy et al., 2010). The study region can be broadly

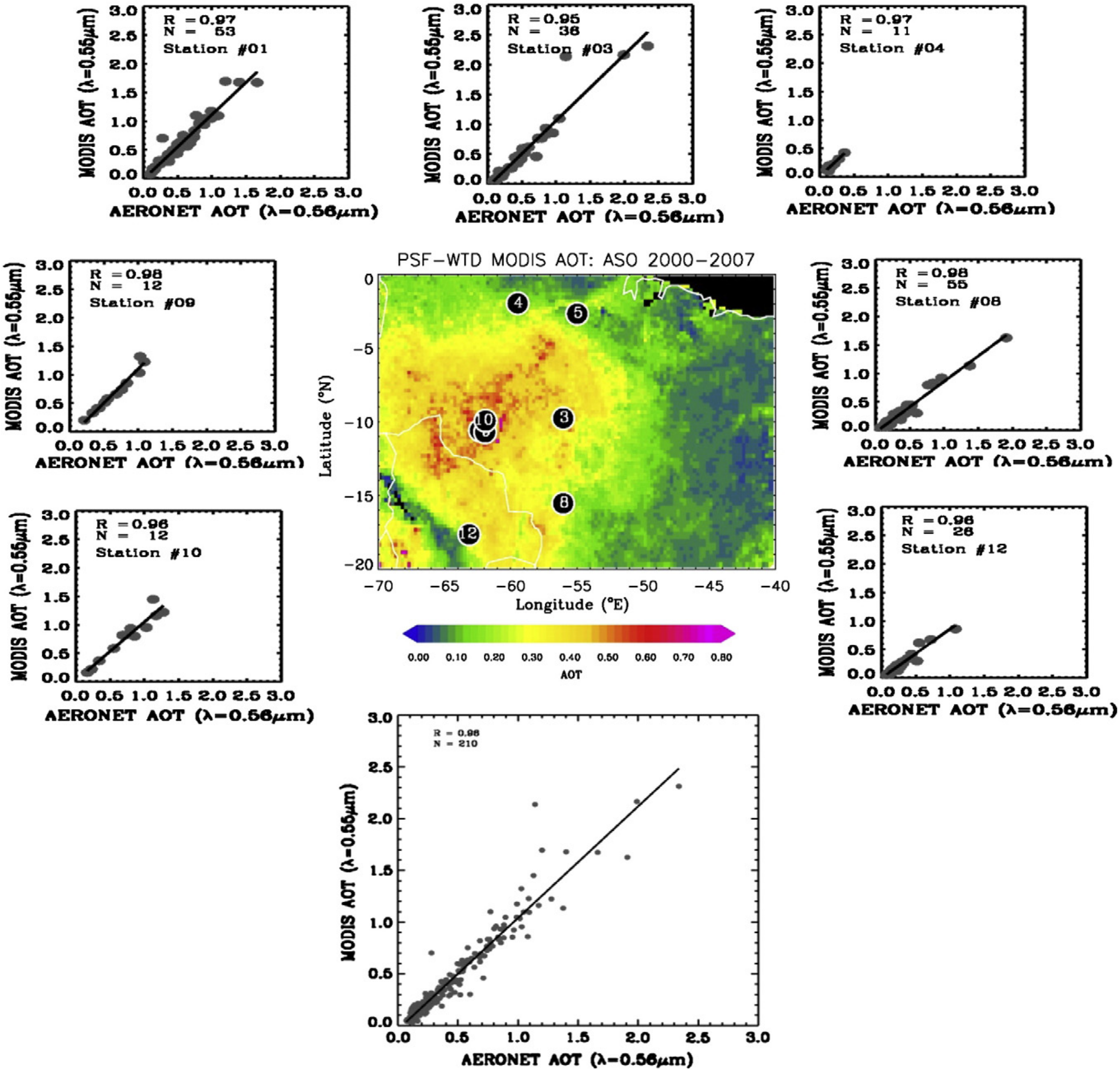

Fig. 1. Comparison of aerosol optical thickness from ground based AERONET instruments and from satellite based MODIS instrument over AERONET stations in South America. The MODIS AOT is point spread AOT over CERES footprint from the CERES–SSF product. The map shows clear sky a composite of AOT in the study region during August–October of 2000–2007.

classified into rainforest, mixed (broadleaf and savanna) and Cerrado (grassland) regions (Prins & Menzel, 1994). The AOT shows a gradient from the west to east with highest AOTs (>0.25) in the rainforest region of the Amazon basin and decreasing AOTs from the Savanna (0.1–0.25) to the Cerrado (<0.1) region. Note that these spatial distributions are rather complex and dependent upon not just aerosol sources but advection due to winds, hygroscopic growth, and other factors. The AOT depends on the concentration, optical and microphysical properties of aerosols (Kaufman et al., 1997; Reid, Eck, et al., 2005; Reid, Koppmann, Eck, & Eleuterio, 2005). The AOT inter-comparisons are shown for all those locations (black dots in the map) for which collocated data was available during the study period. The correlation coefficient (R) value ranging from 0.95 to 0.98 suggests the robustness of the PSF-weighted MODIS AOT (in the CERES product) used in this study. The AOT in the CERES data set is largely from the MODIS collection 4 data with few months (Aug–Oct, 2006–2008) of data from collection 5. The MODIS collection 4 algorithm for aerosol retrieval over land assumes a single aerosol model over entire South America with single scattering albedo value of 0.9 (Remer et al., 2005). This moderately absorbing aerosol model is assumed throughout the year with no seasonal changes. Comparison of MODIS collection 4 with AERONET shows that 72% retrievals over South America falls within the MODIS uncertainty limits with 21% mean difference in MODIS and AERONET AOTs (Remer et al., 2005). However, in collection 5, aerosol models are defined for each season. Also, collection 5 MODIS retrievals make use of absorbing type of aerosols (SSA = 0.85) over south-east of Amazon, but everywhere else it is the same as used in collection 4 data (Levy, Remer, Mattoo, Vermote, & Kaufman, 2007).

3.2. Inter-comparison of shortwave aerosol radiative forcing

In Patadia et al. (2011) a comparison between the shortwave fluxes from the CERES pixel level product and that derived using the empirical angular distribution models (EADMs) showed that the

CERES shortwave flux for AOT below ~0.3 is higher than shortwave flux from EADM and for AOT > 0.3, it is lower. As described in Section 3.1, Fig. 1 shows that AOT > 0.3 pertains to the Amazon region with broadleaf forest area while AOT < 0.3 mostly belongs to the Savanna region. Since the EADMs are characterized by AOT, the difference in shortwave fluxes can be attributed to the AOT; and therefore, region specific smoke angular models are used in this study to convert radiances to fluxes. These differences, however, have implications for the shortwave aerosol

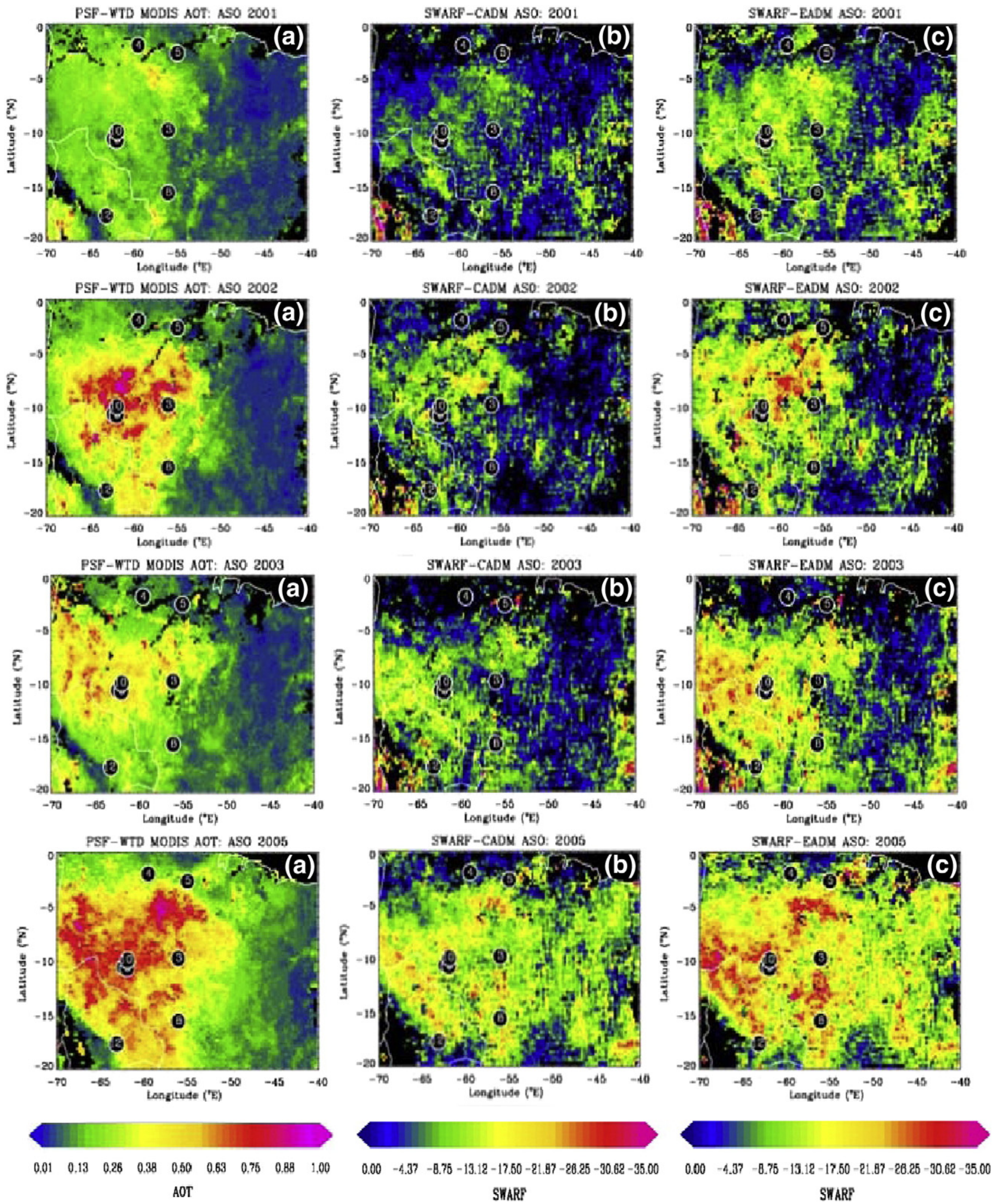

Fig. 2. The three columns show (a) spatial distribution of point spread weighted AOT (b) shortwave aerosol radiative forcing derived from CERES shortwave fluxes and (c) shortwave aerosol radiative forcing derived using shortwave fluxes from empirical angular distribution models in the study region during August–October of 2001–2005 (minus 2004). The SWARF patterns from EADM are in better agreement with the AOT patterns in (a).

radiative forcing (SWARF). To investigate the differences in SWARF from the two datasets, we calculate the cloud-free SWARF using methods described in Section 2 above.

Fig. 2 shows the spatial distribution of AOT (Fig. 2a) and SWARF (Fig. 2b, c) during August–October of 2001–2005. In Fig. 2b the SWARF is derived from CERES shortwave fluxes; and in Fig. 2(c), the SWARF is derived from EADM (Patadia et al., 2011). As described in the previous section, a west to east gradient can be seen in both AOT and SWARF spatial distributions. For all the years, a visual comparison of SWARF from Fig. 2b and c against the AOT map (Fig. 2a) shows that the radiative forcing spatial pattern from EADM is in better agreement with the AOT pattern in Fig. 2a. Also, SWARF from EADM is higher than those obtained from the CERES fluxes since an aerosol scene appears brighter in the shortwave when compared to a clear sky scene without aerosols. The CERES angular distribution models that are constructed for every month and for every 1 × 1 degree latitude–longitude region are region specific and capture the contrast between these two scenes with differing brightness. When a beam of light is incident on aerosol particles suspended in the air, the light is redistributed in all angular directions (Mie scattering) with a dominant lobe in the forward scattering direction. Since the anisotropy in the scattered radiation caused by aerosols is not captured by the CERES ADMs, the magnitude and gradients in the estimated fluxes do not compare well with the AOT. Since the empirical angular distribution models developed in this study pertain to the biomass burning season and are characterized by AOT, the gradients in fluxes and hence the SWARF from EADM fluxes are in better agreement with AOT. This example shows the need to characterize the ADMs with aerosol information such as the AOT.

An inter-comparison of the pixel level SWARF during August–October of 2000–2007 derived from CERES shortwave fluxes (SWARF–CADM) and shortwave fluxes from empirical angular distribution models (SWARF–EADM) is shown in Fig. 3a. The inset shows the frequency distribution (%) of the SWARF–EADM and SWARF–CADM differences. The SWARF–EADM is higher than SWARF–CADM, except over bright regions (surface albedo > 0.16) with low aerosol loading (AOT < 0.03). The relationship of aerosol forcing with AOT from SSF (square) and EADM (solid circles) datasets is shown in Fig. 3b. The insets show the frequency distribution (%) of SWARF–EADM and SWARF–CADM. For the AOT thickness range of 0.0–0.6, Fig. 3b shows that the SWARF from EADM fluxes has a larger slope, which indicates a larger radiative forcing efficiency (defined as the slope of the relation between SWARF and AOT or in other words it is the SWARF per unit optical thickness). It is noted that the clear sky (AOT < 0.1) SWARF from the two datasets is nearly the same. Since the empirical ADMs in this study are characterized by aerosol optical thickness and surface albedo (SALB), differences in SWARF are expected to vary with both parameters. The analysis of the difference in SWARF magnitudes with AOT and surface albedo is shown in Fig. 4. The AOT values in the figure are the center values of AOT bins [0,0.05,0.1,0.15,0.2,0.25,0.3,0.4,0.5,0.6]. Each point in the figure represents the average SWARF difference in AOT and SALB bins [0.1, 0.12, 0.13, 0.14, 0.16, 0.18]. Fig. 4 shows that for SALB and AOT range of the data, SWARF estimated using fluxes from EADM (SWARF EADM) is greater than the SWARF estimated from CERES SSF shortwave fluxes (SWARF CADM). This SWARF difference increases with increase in AOT. Since the EADMs used to derive fluxes are characterized by AOT, the differences are expected to increase with increase in AOT. For AOT values ≤0.1, the difference is ≤2 Wm^{-2} and increases to between ≤5 Wm^{-2} for AOT ≤ 0.3. When AOT is ≥0.3, the difference is between 5 and 10 Wm^{-2}. In Patadia et al. (2011), we found that for AOT less (more) than 0.3, the shortwave flux from EADM was less (higher) than the CERES SSF shortwave flux. This is attributed to the differences in aerosol information used in estimating the anisotropic factors (Zhang et al., 2005a). From Fig. 4, it is also noted that, in all the AOT bins, the differences are larger (smaller) when SALB is low (high). For example, for 0.1 < SALB < 0.12 the SWARF difference ranges between 1 and 10 Wm^{-2} while the range decreases to 0.5–6 Wm^{-2} when SALB > 0.16. This variation in SWARF differences with respect to surface albedo could be attributed to the following. For a given aerosol type (e.g. constant single scattering albedo), the contrast between the surface and the aerosol field governs its radiative effect (see Patadia, Yang, & Christopher, 2009 and references therein). When the surface is brighter (darker), then the radiative effect of a given aerosol is smaller (larger). For example over a densely vegetated area, the aerosol forcing is higher since the contrast between the surface and aerosol is high. Therefore, over a given geographic region, the changes in both surface and aerosol characteristics are important to aerosol radiative forcing. If the radiative fluxes used for estimating SWARF do not account for the aerosols, the uncertainty associated

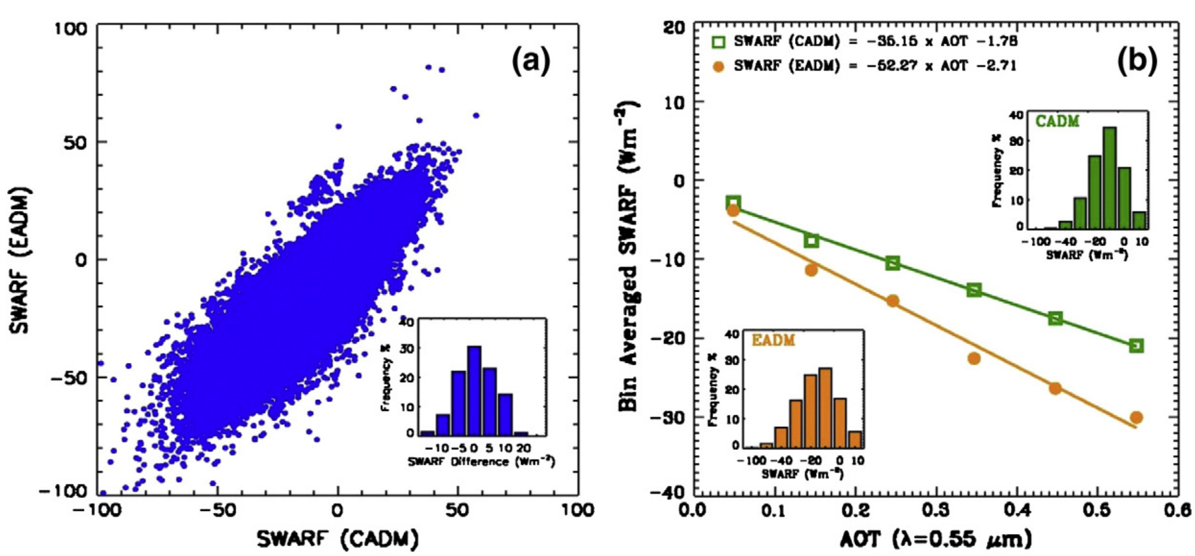

Fig. 3. A comparison of the pixel level shortwave aerosol radiative forcing during August–October of 2000–2007 derived from CERES shortwave fluxes (SWARF–SSF) and shortwave fluxes derived using empirical angular distribution models (SWARF–EADM). Inset shows the frequency distribution (%) of the difference in EADM and CADM SWARFs. (b) Comparison of the SWARF–AOT relation from CADM (square) and EADM (solid circles) datasets. Insets show the frequency distribution (%) of the SWARFs from EADM and CADM. This figure shows the implication of the differences in SWARF from the two datasets. The larger slope of SWARF from EADM fluxes indicates a larger radiative forcing efficiency.

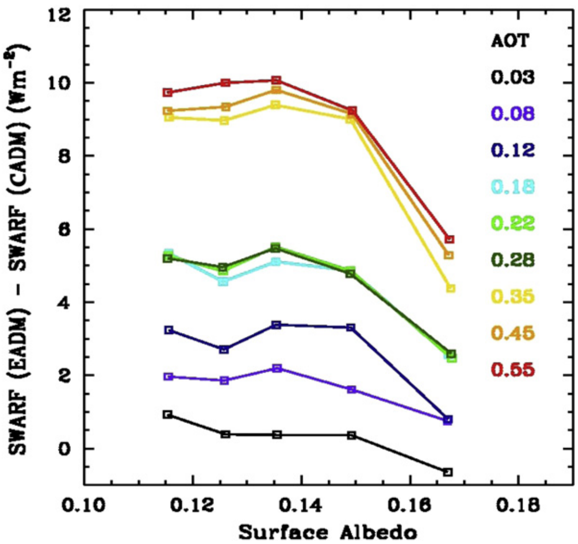

Fig. 4. Difference between shortwave aerosol forcing from fluxes derived using empirical angular distribution models (SWARF EADM) and shortwave aerosol forcing derived using CERES SSF shortwave flux data (SWARF CADM) as a function of surface albedo (x-axis) and aerosol optical thickness (in different colors). The AOT values in the figure are the center values of AOT bins [0,0.05,0.1,0.15,0.2,0.25,0.3,0.4,0.5,0.6]. Each point in the figure represents the average SWARF difference in a AOT and SALB bins [0.1, 0.12, 0.13, 0.14, 0.16, 0.18].

with SWARF estimates at higher AOT is larger and the gradients in SWARF may not be representative. In such cases, the confidence in inferring the implications of the SWARF to regional hydrological cycle and climate is challenging.

3.3. Comparison with previous studies

In this section we report SWARF of biomass burning aerosols from previous studies. The only study thus far that has addressed SWARF of biomass burning aerosols using angular models is by Li et al. (2000) that was based on radiative transfer calculations. Based on the measurement from SCAR-B experiment, Li et al. (2000) constructed smoke ADMs using discrete ordinate radiative transfer model and applied them to calculate TOA radiative fluxes in shortwave. They found a root mean square RMS error of 13 Wm^{-2} between the existing CERES SW fluxes (that used ERBE ADMs) and the fluxes estimated using their smoke ADM with a relative error in SWARF estimates of <10%. The CERES angular models used for calculating TOA fluxes have matured substantially when compared to the ERBE approach. However, as noted before, these angular models do not account for aerosols over land. From the new empirical smoke ADMs in this study, we find that the CERES derived SWARF is underestimated by ~3.3 Wm−^{2} when compared to SWARF derived from the fluxes using our EADMs.

Table 2 shows a listing of various studies that have reported the TOA SWARF over regions with biomass burning aerosols using combined narrowband and broadband satellite observations as used in our study. We note that it is sometimes difficult to compare our results with previous work because the areas of the study are different and the SWARF is not calculated in the same way. Also, our EADMs that are used to convert the shortwave radiances to flux are characterized for AOT $\leq$ 0.6 and therefore the shortwave radiative fluxes as well as the SWARF are limited to AOT ranging from 0.0 to 0.6 only. A more complete comparison should include all ranges of AOT. However, from Table 2, we find that the 24-hour mean forcing from different studies generally ranges from −4 to −34 Wm^{-2} while AOTs vary between 0.1 and 1.2. In this study, we find that the mean SWARF (for AOT = 0.0–0.6) from CERES is −8.1 ± 4.2 while the SWARF from EADM fluxes is −11.4 ± 4.9 (see Table 1). Since the AOT ranges vary from one study to another, including in our study, a better comparison would be that of the forcing per unit AOT at 550 nm here also known as the radiative forcing efficiency. This is the slope between SWARF and AOT. The mean AOT reported in Table 1 for this study is the mean of the range of AOT (0.0–0.6) for which EADMs are constructed. From Table 2 we find that the efficiency from various studies has a range from −22 to −45 Wm$^{-2}\tau^{-1}$ with a mean of −34 ± 8 Wm$^{-2}\tau^{-1}$. From 8 years (2000–2008) analysis, the forcing per unit AOT (or efficiency) in our study is found to be −35.2 ± 7.8 and −52.3 ± 8.0 Wm$^{-2}\tau^{-1}$ from CERES and EADM fluxes respectively (see Fig. 3). We anticipate similar differences in the efficiencies from the two data sets even if the entire range of AOT was used. Li et al. (2000) used VIRS/TRMM and CERES observations over the Amazon region and reported the instantaneous forcing efficiency of −29 Wm$^{-2}\tau^{-1}$at 0.55 μm (Table 2). For a 1998 biomass burning episode in Central America, Christopher, Li, et al. (2000) used VIRS/TRMM and CERES observations and estimated the 24-hour mean aerosol radiative forcing efficiency of −36 Wm$^{-2}\tau^{-1}$ at 0.55 μm. The 24-hour mean radiative forcing efficiency of biomass burning aerosols outflow from South Africa was reported to be −45 Wm$^{-2}\tau^{-1}$. Comparison of our results with previous studies indicates that the various studies listed in Table 2 that used ERBE or CERES fluxes have a forcing efficiency (−34 ± 8 Wm$^{-2}\tau^{-1}$) similar to what is derived in this study from the CERES fluxes (35.2 ± 7.8 Wm$^{-2}\tau^{-1}$). Since the ADMs used in ERBE or CERES do not account for anisotropy due to scattering from aerosols, the forcing or the forcing efficiency is underestimated.

4. Summary and conclusion

This paper focuses on deriving the impact of smoke ADMs on TOA shortwave aerosol radiative forcing. For this, we calculate the TOA shortwave aerosol radiative forcing during the biomass burning season in South America using TOA (1) CERES shortwave radiative flux observations and (2) shortwave radiative flux derived using empirical smoke angular distribution models developed in Patadia et al. (2011). For the dry season during which biomass burning is at peak (August–October) in South America, an inter-comparison of 8 years (2000–2008) of

Table 1
Summary of instantaneous SWARF estimated from CERES SSF and EADM.

Year	Data points	AOT	Fclr_CADM	Fclr_EADM	SWF_CADM	SWF_EADM	SWARF_CADM	SWARF_EADM
2000	52552	0.18 ± 0.15	157.3 ± 11.4	151.2 ± 12.6	165.2 ± 13.3	163.8 ± 14.9	−7.8 ± 10.8	−11.5 ± 13.2
2001	173202	0.15 ± 0.12	149.1 ± 10.9	143.7 ± 11.6	156.6 ± 13.4	155.6 ± 15.0	−7.5 ± 10.2	−11.0 ± 12.6
2002	158007	0.16 ± 0.14	148.3 ± 9.9	143.3 ± 10.5	157.5 ± 14.5	157.1 ± 16.2	−9.2 ± 12.9	−12.8 ± 15.1
2003	175283	0.17 ± 0.14	150.8 ± 10.9	146.3 ± 10.9	159.6 ± 14.6	159.1 ± 15.8	−8.8 ± 12.3	−11.8 ± 14.0
2004	21464	0.09 ± 0.09	166.8 ± 9.5	161.3 ± 8.9	175.7 ± 15.4	172.8 ± 15.9	−8.9 ± 14.4	−10.4 ± 15.3
2005	220719	0.19 ± 0.15	154.9 ± 9.7	149.5 ± 9.8	164.1 ± 14.0	164.2 ± 15.9	−9.1 ± 11.8	−13.6 ± 14.2
2006	201161	0.14 ± 0.15	150.2 ± 9.9	144.5 ± 10.4	156.4 ± 13.5	154.7 ± 15.2	−6.1 ± 10.9	−9.3 ± 13.4
2007	85674	0.18 ± 0.17	149.7 ± 10.4	143.7 ± 10.4	156.8 ± 12.4	155.6 ± 13.7	−7.2 ± 9.9	−10.9 ± 12.6
Mean	136008	0.16 ± 0.05	153.4 ± 2.8	147.9 ± 3.9	161.5 ± 4.9	160.4 ± 5.5	−8.1 ± 4.2	−11.4 ± 4.9

Table 2
Top of atmosphere cloud-free shortwave aerosol radiative forcing from combined narrowband and broadband satellite observations.

Reference	Area of study	Data used/time period/field experiment	SWARF (Wm^{-2})	AOT and reported wavelength (μm)	Forcing efficiency ($Wm^{-2}\tau^{-1}$)	SWARF Averaging method
Christopher et al. (1996)	Amazon	AVHRR/ERBE 11 images, Aug–Sep 1995	−36	Not reported	No AOT reported	Over pass
Christopher, Wang, Berendes, Welch, & Yang (1998)	Amazon	AVHRR/ERBE Aug–Oct, 1985	−26 to −33	Not reported	No AOT reported	Over pass
Li et al. (2000)[1]	Amazon	VIRS/TRMM–CERES August 1998	−22	1.0	$-22/\tau^{1}_{0.63}$ $(-29/\tau_{0.55})^{2}$	Over pass
Christopher, Chou, et al., 2000	C. America & Gulf of Mexico	VIRS/CERES 4 days, May, 1998	−34	1.2 (0.63)[a]	$-28/\tau^{3}_{0.63}$ $(^{-}36/\tau_{0.55})$	24 h mean
Christopher & Zhang (2002)	South Africa outflow Biomass burning	MODIS/CERES–Terra September, 2000	−12.7	0.14 (0.55)	$-45/\tau_{0.55}$	24 h mean[3]
Loeb & Kato (2002)	Gulf of Mexico	VIRS/TRMM-CERES Jan–Aug, 1998& Mar 2000	−32	1.0 (0.63)	$-32/\tau_{0.63}$ $(-41/\tau_{0.55})^{2}$	24 h mean
Satheesh & Ramanathan (2000)	Kaashidhoo, India	Surface AOT/TRMM–CERES Jan–Mar, 1998&1999	−10	0.41 (0.50)	$-25/\tau_{0.50}$	24 h mean
Rajeev & Ramanathan (2001)	Tropical Indian Ocean	AVHRR/TRMM-CERESJan–Mar, 1997–1999/INDOEX	NH: −4 to −14 SH: 0 to 6	>0.2 < 0.2 (0.63)	$-24/\tau_{0.50}$	24 h mean
Markowicz, Flatau, Ramana, Crutzen, & Ramanathan (2002)	Eastern shores, Greece	Sunphotometer/Terra–CERES/ MINOS experiment, Jul-Aug, 2001	−6.6 ± 2.1	0.21 (0.5)	$-31/\tau_{0.50}$	24 h mean
Zhang et al. (2005b)	South Atlantic Ocean (SAO) Indian Ocean (IO)	Terra–MODIS/CERES Nov–Dec, 2000 and Jan–Feb 2001	SAO: −4.1 IO: −5.3	0.11 0.15 (0.5)	$-37/\tau^{3}_{0.55}$ $-35/\tau_{0.55}$	24 h mean
Patadia et al. (2008)	Amazon	Terra–MISR/CERES Aug–Sep, 2000–2006	−7.6	0.24	$-44.2/\tau_{0.55}$	24 h mean

Note: 24 h mean SWARF is ~0.5 of the instantaneous SWARF (Patadia et al., 2008; Remer & Kaufman, 2006).
[a] Value in parentheses is the forcing efficiency at 0.55 μm wavelength.

SWARF–CADM (-8.1 ± 4.2 Wm^{-2}) and SWARF–EADM (-11.4 ± 4.9 Wm^{-2}) shows that the instantaneous SWARF is underestimated by ~3.3 Wm^{-2} if the ADMs used to convert the shortwave radiances to flux do not account for aerosols. During the biomass burning season, a high concentration of smoke aerosols in South America contributes considerably to the anisotropy in the scattered radiation and therefore should not be ignored while developing angular distribution models. A ten-year data set from Terra–CERES is now available that can be used to build empirical angular models characterized by aerosols over global land areas similar to the work by Zhang et al. (2005a) for global oceans.

References

Ackerman, A. S., Toon, O. B., Stevens, D. E., Heymsfield, A. J., Ramanathan, V., & Welton, E. J. (2000). Reduction of tropical cloudiness by soot. *Science*, *288*, 1042–1047.

Andreae, M.O., Artaxo, P., Fischer, H., Freitas, S. R., Grégoire, J. M., Hansel, A., et al. (2001). Transport of biomass burning smoke to the upper troposphere by deep convection in the equatorial region. *Geophysical Research Letters*, *28*, 951–954.

Bergstrom, R. W., Pilewskie, P., Schmid, B., & Russell, P. B. (2003). Estimates of the spectral aerosol single scattering albedo and aerosol radiative effects during SAFARI 2000. *Journal of Geophysical Research-Atmospheres*, *108*, 8474.

Bevan, S. L., North, P. R. J., Grey, W. M. F., Los, S. O., & Plummer, S. E. (2009). Impact of atmospheric aerosol from biomass burning on Amazon dry-season drought. *Journal of Geophysical Research-Atmospheres*, *114*, D09204.

CCSP (2009). Atmospheric aerosol properties and impacts on climate, a report by the U.S.Climate Change Science Program and the Subcommittee on Global Change Research. In M. Chin, R. A. Kahn, & S. E. Schwartz (Eds.), Washington, D.C., USA: National Aeronautics and Space Administration (128 pp.).

Christopher, S. A., Chou, J., Zhang, J., Li, X., Berendes, T. A., & Welch, R. M. (2000). Shortwave direct radiative forcing of biomass burning aerosols estimated using VIRS and CERES data. *Geophysical Research Letters*, *27*, 2197–2200.

Christopher, S. A., Kliche, D.V., Chou, J., & Welch, R. M. (1996). First estimates of the radiative forcing of aerosols generated from biomass burning using satellite data. *Journal of Geophysical Research D: Atmospheres*, *101*, 21265–21273.

Christopher, S. A., Li, X., Welch, R. M., Reid, J. S., Hobbs, P. V., Eck, T. F., et al. (2000). Estimation of surface and top-of-atmosphere shortwave irradiance in biomass-burning regions during SCAR-B. *Journal of Applied Meteorology*, *39*, 1742–1753.

Christopher, S. A., Wang, M., Berendes, T. A., Welch, R. M., & Yang, S. -K. (1998). The 1985 biomass burning season in South America: Satellite remote sensing of fires, smoke, and regional radiative energy budgets. *Journal of Applied Meteorology*, *37*, 661–678.

Christopher, S. A., & Zhang, J. (2002). Shortwave aerosol radiative forcing from MODIS and CERES observations over the oceans. *Geophysical Research Letters*, *29*, 1859.

Crutzen, P. J., & Andreae, M.O. (1990). Biomass burning in the tropics: Impact on atmospheric chemistry and biogeochemical cycles. *Science*, *250*, 1669–1678.

Geier, E. B., Green, R. N., Kratz, D. P., Minnis, P., Miller, W. F., Nolan, S. K., et al. (2001). Single satellite footprint TOA/surface fluxes and clouds (SSF) collection document. Available online from. http://asd-www.larc.nasa.gov/ceres/ASDceres.html

Gupta, P., Patadia, F., & Christopher, S. A. (2008). Multisensor data product fusion for aerosol research. *IEEE Transactions on Geoscience and Remote Sensing*, *46*, 1407–1415.

Guyon, P., Frank, G. P., Welling, M., Chand, D., Artaxo, P., Rizzo, L., et al. (2005). Airborne measurements of trace gas and aerosol particle emissions from biomass burning in Amazonia. *Atmospheric Chemistry and Physics*, *5*, 2989–3002.

Hao, W. M., & Liu, M. -H. (1994). Spatial and temporal distribution of tropical biomass burning. *Global Biogeochemical Cycles*, *8*, 495–503.

Haywood, J., & Boucher, O. (2000). Estimates of the direct and indirect radiative forcing due to tropospheric aerosols: A review. *Reviews of Geophysics*, *38*, 513–543.

Iacobellis, S. F., Frouin, R., & Somerville, R. C. J. (1999). Direct climate forcing by biomass-burning aerosols: Impact of correlations between controlling variables. *Journal of Geophysical Research D: Atmospheres*, *104*, 12031–12045.

Ichoku, C., Remer, L. A., Kaufman, Y. J., Levy, R., Chu, D. A., Tanré, D., et al. (2003). MODIS observation of aerosols and estimation of aerosol radiative forcing over southern Africa during SAFARI 2000. *Journal of Geophysical Research*, *108*, 8499.

IPCC Climate Change (2007). Climate change 2007: The physical science basis. In S. Solomon, D. Qin, M. Manning, Z. Chan, M. Marquis, K. B. Averty, & H. L. Miller (Eds.), Cambridge, U.K.: Cambridge University Press.

Ito, A., & Penner, J. E. (2004). Global estimates of biomass burning emissions based on satellite imagery for the year 2000. *Journal of Geophysical Research*, *109*, D14S05.

Jones, T. A., & Christopher, S. A. (2010). Statistical properties of aerosol-cloud-precipitation interactions in South America. *Atmospheric Chemistry and Physics*, *10*, 2287–2305.

Kaufman, Y. J., & Fraser, R. S. (1997). The Effect of smoke particles on clouds and climate forcing. *Science*, *277*, 1636–1639.

Kaufman, Y. J., Holben, B. N., Tanré, D., Slutsker, I., Smirnov, A., & Eck, T. F. (2000). Will aerosol measurements from Terra and Aqua Polar Orbiting satellites represent the daily aerosol abundance and properties? *Geophysical Research Letters*, *27*, 3861–3864.

Kaufman, Y. J., Tanré, D., Remer, L. A., Vermote, E. F., Chu, A., & Holben, B. N. (1997). Operational remote sensing of tropospheric aerosol over land from EOS moderate resolution imaging spectroradiometer. *Journal of Geophysical Research D: Atmospheres*, *102*, 17051–17067.

Koch, D., Bond, T. C., Streets, D., & Unger, N. (2007). Linking future aerosol radiative forcing to shifts in source activities. *Geophysical Research Letters*, *34*.

Koren, I., Kaufman, Y. J., Remer, L. A., & Martins, J. V. (2004). Measurement of the effect of Amazon smoke on inhibition of cloud formation. *Science*, *303*, 1342–1345.

Levy, R. C., Remer, L. A., Kleidman, R. G., Mattoo, S., Ichoku, C., Kahn, R., et al. (2010). Global evaluation of the Collection 5 MODIS dark-target aerosol products over land. *Atmospheric Chemistry and Physics*, *10*, 14815–14873.

Levy, R. C., Remer, L. A., Mattoo, S., Vermote, E. F., & Kaufman, Y. J. (2007). Second-generation operational algorithm: Retrieval of aerosol properties over land from inversion of Moderate Resolution Imaging Spectroradiometer spectral reflectance. *Journal of Geophysical Research*, *112*, D13211.

Li, X., Christopher, S. A., Chou, J., & Welch, R. M. (2000). Estimation of shortwave direct radiative forcing of biomass-burning aerosols using new angular models. *Journal of Applied Meteorology*, *39*, 2278–2291.

Loeb, N. G., & Kato, S. (2002). Top-of-atmosphere direct radiative effect of aerosols over the tropical oceans from the Clouds and the Earth's Radiant Energy System (CERES) satellite instrument. *Journal of Climate*, *15*, 1474–1484.

Loeb, N. G., & Manalo-Smith, N. (2005). Top-of-atmosphere direct radiative effect of aerosols over global oceans from merged CERES and MODIS observations. *Journal of Climate*, *18*, 3506–3526.
Marengo, J. A., Jones, R., Alves, L. M., & Valverde, M. C. (2009). Future change of temperature and precipitation extremes in South America as derived from the PRECIS regional climate modeling system. *International Journal of Climatology*, *29*, 2241–2255.
Markowicz, K. M., Flatau, P. J., Ramana, M. V., Crutzen, P. J., & Ramanathan, V. (2002). Absorbing mediterranean aerosols lead to a large reduction in the solar radiation at the surface. *Geophysical Research Letters*, *29*, 1968.
Moraes, E. C., Franchito, S. H., & Brahmananda Rao, V. (2004). Effects of biomass burning in Amazonia on climate: A numerical experiment with a statistical-dynamical model. *Journal of Geophysical Research D: Atmospheres*, *109*(D05109), 05101–05112.
Patadia, F., Christopher, S. A., & Zhang, J. (2011). Development of empirical angular distribution models for smoke aerosols: Methods. *Journal of Geophysical Research*, *116*, D14203.
Patadia, F., Gupta, P., Christopher, S. A., & Reid, J. S. (2008). A Multisensor satellite-based assessment of biomass burning aerosol radiative impact over Amazonia. *Journal of Geophysical Research*, *113*, D12214.
Patadia, F., Yang, E. -S., & Christopher, S. A. (2009). Does dust change the clear sky top of atmosphere shortwave flux over high surface reflectance regions? *Geophysical Research Letters*, *36*, L15825.
Prins, E. M., Feltz, J. M., Menzel, W. P., & Ward, D. E. (1998). An overview of GOES-8 diurnal fire and smoke results for SCAR-B and 1995 fire season in South America. *Journal of Geophysical Research*, *103*, 31821–31835.
Prins, E. M., & Menzel, W. P. (1994). Trends in South American biomass burning detected with the GOES visible infrared spin scan radiometer atmospheric sounder from 1983 to 1991. *Journal of Geophysical Research*, *99*, 16719–16735.
Procopio, A. S., Artaxo, P., Kaufman, Y. J., Remer, L. A., Schafer, J. S., & Holben, B. N. (2004). Multiyear analysis of amazonian biomass burning smoke radiative forcing of climate. *Geophysical Research Letters*, *31*, L03108.
Rajeev, K., & Ramanathan, V. (2001). Direct observations of clear-sky aerosol radiative forcing from space during the Indian Ocean Experiment. *Journal of Geophysical Research*, *106*, 17221–17235.
Reid, J. S., Eck, T. F., Christopher, S. A., Koppmann, R., Dubovik, O., Eleuterio, D. P., et al. (2005). A review of biomass burning emissions part III: Intensive optical properties of biomass burning particles. *Atmospheric Chemistry and Physics*, *5*, 827–849.
Reid, J. S., Hobbs, P. V., Rangno, A. L., & Hegg, D. A. (1999). Relationships between cloud droplet effective radius, liquid water content, and droplet concentration for warm clouds in Brazil embedded in biomass smoke. *Journal of Geophysical Research*, *104*, 6145–6153.
Reid, J. S., Koppmann, R., Eck, T. F., & Eleuterio, D. P. (2005). A review of biomass burning emissions part II: Intensive physical properties of biomass burning particles. *Atmospheric Chemistry and Physics*, *5*, 799–825.
Remer, L. A., & Kaufman, Y. J. (2006). Aerosol direct radiative effect at the top of the atmosphere over cloud free ocean derived from four years of MODIS data. *Atmospheric Chemistry and Physics*, *6*, 237–253.
Remer, L. A., Kaufman, Y. J., Tanré, D., Mattoo, S., Chu, D. A., Martins, J. V., et al. (2005). The MODIS aerosol algorithm, products, and validation. *Journal of the Atmospheric Sciences*, *62*, 947–973.
Rosenfeld, D., & Woodley, W. L. (2000). Deep convective clouds with sustained supercooled liquid water down to −37.5 °C. *Nature*, *405*, 440–442.
Ross, J. L., Hobbs, P. V., & Holben, B. (1998). Radiative characteristics of regional hazes dominated by smoke from biomass burning in Brazil: Closure tests and direct radiative forcing. *Journal of Geophysical Research*, *103*, 31925–31941.
Satheesh, S. K., & Ramanathan, V. (2000). Large differences in tropical aerosol forcing at the top of the atmosphere and Earth's surface. *Nature*, *405*, 60–63.
Vermote, E., Ellicott, E., Dubovik, O., Lapyonok, T., Chin, M., Giglio, L., et al. (2009). An approach to estimate global biomass burning emissions of organic and black carbon from MODIS fire radiative power. *Journal of Geophysical Research-Atmospheres*, *114*, D18205.
Wielicki, B.A., Barkstrom, B. R., Harrison, E. F., Lee, R. B., Louis Smith, G., & Cooper, J. E. (1996). Clouds and the Earth's Radiant Energy System (CERES): An Earth Observing System experiment. *Bulletin of the American Meteorological Society*, *77*, 853–868.
Yu, H., Kaufman, Y. J., Chin, M., Feingold, G., Remer, L. A., Anderson, T. L., et al. (2006). A review of measurement-based assessments of the aerosol direct radiative effect and forcing. *Atmospheric Chemistry and Physics*, *6*, 613–666.
Zhang, J., Christopher, S. A., Remer, L. A., & Kaufman, Y. J. (2005a). Shortwave aerosol radiative forcing over cloud-free oceans from Terra: 1. Angular models for aerosols. *Journal of Geophysical Research*, *110*, D10S23.
Zhang, J., Christopher, S. A., Remer, L. A., & Kaufman, Y. J. (2005b). Shortwave aerosol radiative forcing over cloud-free oceans from Terra: 2. Seasonal and global distributions. *Journal of Geophysical Research*, *110*, D10S24.
Zhang, Y., Fu, R., Yu, H., Qian, Y., Dickinson, R., Dias, M.A. F. S., et al. (2009). Impact of biomass burning aerosol on the monsoon circulation transition over Amazonia. *Geophysical Research Letters*, *36*.